COMMUNICATIONS CHEMISTRY

ARTICLE

DOI: 10.1038/s42004-018-0018-y OPEN

Adaptive aromaticity in S_0 and T_1 states of pentalene incorporating 16 valence electron osmium

Dandan Chen[1], Ting Shen[1], Ke An[1] & Jun Zhu[1]

Aromaticity is a fundamental chemical concept of ever-increasing diversity. According to Hückel's and Baird's rules, cyclic conjugated species with $4n+2$ π-electrons are aromatic in the singlet electronic ground state (S_0) and antiaromatic in the lowest triplet state (T_1), and vice-versa. Thus, species with aromaticity in both states have not yet been reported. Here we carry out density functional theory calculations on recently synthesized organometallics, namely osmapentalyne and osmapentalenes, and demonstrate the first example (16-electron osmapentalene) of aromaticity in both S_0 and T_1 states, which we term adaptive aromaticity. Further electronic structure analysis reveals that the excitation pattern for the formation of the T_1 state plays a crucial role in the achievement of adaptive aromaticity. Our findings highlight the role of a transition metal in unorthodox excitation behavior, and may aid the design of adaptive aromatics for photochemical and molecular magnetism applications.

[1] State Key Laboratory of Physical Chemistry of Solid Surfaces and Collaborative Innovation Center of Chemistry for Energy Materials (iChEM), Fujian Provincial Key Laboratory of Theoretical and Computational Chemistry and Department of Chemistry, College of Chemistry, and Chemical Engineering, Xiamen University, Xiamen 361005, China. Correspondence and requests for materials should be addressed to J.Z. (email: jun.zhu@xmu.edu.cn)

Aromaticity has been one of the most important concepts in chemistry since the discovery of benzene in 1825. The classical [4*n*+2] rule to rationalize aromaticity was first proposed by Erich Hückel in 1931 and was later developed by Doering[1,2]. In 1960s, Dewar gave the first explanation on Hückel's rule, which was later extended to Möbius topology by Heilbronner and Zimmerman but inverted[3–6]. The concept of ground-state aromaticity has been well developed and serves as a robust tool for rationalizing chemical reactions and properties[7,8].

Excited-state aromaticity[9–12] can be traced back to 1972, when Baird proposed that the aromaticity of planar annulenes in the S_0 state should be reversed in the T_1 state[13], which was later applied to both Hückel and Möbius topologies by Aihara[14]. Experimentally, Wan and co-workers reported the formation of a 4π aromatic intermediate (or transition state) in a photosolvolysis reaction[15]. Schleyer and co-workers supported Baird's rule by theoretical investigation of aromaticity in 4$n\pi$ annulenes in their singlet and triplet states[16]. Recently, Kim and Osuka characterized the excited-state (anti)aromaticity in expanded porphyrins[17–22]. Ottosson and co-workers reported a series of "aromatic chameleons" that are prone to be aromatic in both the T_1 and S_1 states[23–27]. Note that Baird's rule can also be applied to the S_1 state[28–30]. Recently, Xia and co-workers synthesized several novel aromatic osmapentalynes and osmapentalenes[31,32]. Through density functional theory (DFT) calculations, we revealed that these organometallics exhibit Craig-type Möbius aromaticity resulting from eight-center eight-electron (8c–8e) d_π-p_π conjugation. Note that such Craig-type Möbius aromaticity was computationally demonstrated in 4$n\pi$ planar metallacycles early in 2010 by Mauksch and Tsogoeva[33] and in osmasilapentalyne[34] and dimetalla[10] annulenes by us[35]. However, the aromaticity of these novel organometallics in the excited-state has not been reported so far. Despite these extensive studies on aromaticity, to date no example has been reported to be aromatic in both the S_0 and T_1 (or S_1) states. Here we demonstrate the first example, to the best of our knowledge, of a complex with aromaticity in both the S_0 and T_1 states, termed as adaptive aromaticity. This is supported by DFT calculations on simplified model complexes (verified in our previous studies) to examine aromaticity in their T_1 states.

Results

The geometries of model complexes 1–3. We first examined the geometries of model complexes **1**–**3** (Fig. 1a) in both the S_0 and the T_1 states. As shown in Fig. 1b, the C–C bond lengths of these complexes in the S_0 state are in the range of 1.371–1.414 Å, which are much longer than a double bond (1.329 Å in CH_2=CH_2) and significantly shorter than a single bond (1.531 Å in CH_3–CH_3) calculated at the same level of theory, revealing highly delocalized C–C bonds and thus suggesting their aromaticity. In sharp contrast, the bond length alternations (BLAs) in their T_1 states are 0.071, 0.016, and 0.066 Å, suggesting a distinctive difference of complex **2** among these three complexes. In line with the BLAs, the harmonic oscillator model of aromaticity (HOMA) value of complex **2** in the T_1 state (0.950) is quite larger than those of the other two complexes (0.721 for **1** and 0.801 for **3**). The particularly small difference of HOMA values (ΔHOMA, 0.006, Supplementary Table 1) between the S_0 and T_1 states in complex **2** suggests its triplet-state aromaticity.

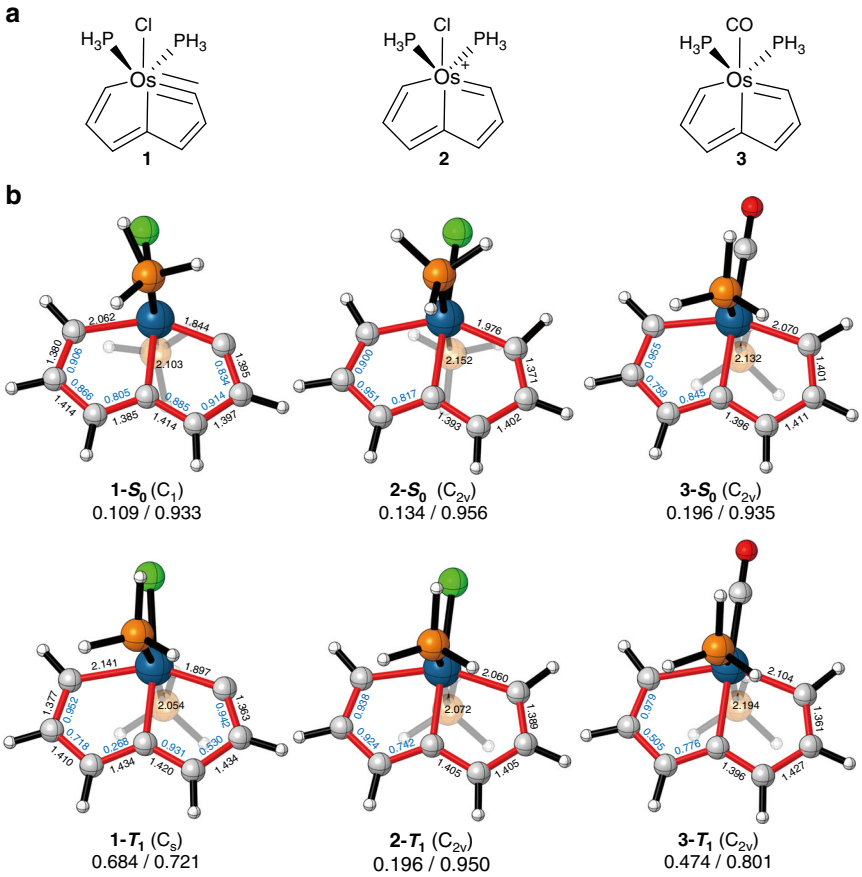

Fig. 1 ELF$_\pi$ bifurcation values and HOMA values of osmium complexes **1**–**3**. **a** The structures of complexes **1**–**3**. **b** BV(ELF$_\pi$)s (blue) and bond lengths (Å, black) are annotated along the bonds. Values before and after the slash "/" correspond to ΔBV(ELF$_\pi$) and HOMA values, respectively

Aromaticity analyses based on magnetic properties. To further evaluate the (anti)aromaticity of these osmacycles, we performed the nucleus-independent chemical shift (NICS) calculations in both their S_0 and the T_1 states[36,37], two-dimensional NICS grids are capable to display the magnetic shielding in aromatic rings and de-shielding in antiaromatic rings[38,39]. Compared with other NICS indices, the NICS(1)$_{zz}$ is chosen here as it can be easily computed and also highly effective in evaluating π aromaticity in both the S_0 and the T_1 states[40,41]. All these complexes in the S_0 state (**1**-S_0, **2**-S_0, and **3**-S_0) and complex **2** in the T_1 state (**2**-T_1) are aromatic, according to the significantly negative (shielded) NICS(1)$_{zz}$ values in these osmacycles (Fig. 2a–c, e). On the contrary, complex **1** in the T_1 state (**1**-T_1) shows antiaromaticity indicated by the highly positive NICS(1)$_{zz}$ values inside the rings (Fig. 2d). Complex **3** in the T_1 state (**3**-T_1), however, does not show either shielding or de-shielding effects at the ring centers, thus suggesting its nonaromaticity (Fig. 2f). In comparison, the NICS grids of benzene and pentalene in the T_1 state (Supplementary Fig. 2) reveal their antiaromaticity and aromaticity, respectively. Note that NICS scans for complexes **1**–**3** in the S_0 and T_1 states in Supplementary Fig. 3 further support the reliability of choosing NICS(1)$_{zz}$.

To further verify the (anti)aromaticity of these complexes, we computed the anisotropy of the induced current density (ACID) for these complexes (Fig. 3), which can provide intuitive pictures showing the induced currents caused by an external magnetic field[42,43]. Clockwise currents along the perimeter of the fused rings in **1**-S_0, **2**-S_0, **3**-S_0, and **2**-T_1 indicate aromaticity, in line with the NICS grids. In sharp contrast, the ring current in **1**-T_1 is anti-clockwise, characteristic of antiaromaticity. The current density vectors in **3**-T_1 are tiny and in disorder, supporting its nonaromaticity (Fig. 3).

Aromaticity analyses based on electron localization function. In general, it is much safer to draw a conclusion on aromaticity based on different physicochemical properties. Topological analyses of the electron localization function (ELF)[44], and in particular the π-contribution, ELF$_\pi$, is an excellent tool to directly link molecular electronic structure properties with (anti)aromaticity[45,46]. Thus, we carried out ELF$_\pi$ analysis to examine the delocalization of π electrons along the perimeter of osmacycles. The π orbitals were taken from our previous calculations, which are responsible for Möbius aromaticity resulting from 8c–8e d_π-p_π conjugation (Supplementary Fig. 4). According to the previous study on a series of polybenzenoid hydrocarbons, the ELF$_\pi$ bifurcation values (BV(ELF$_\pi$)s) in the range of 0.65–0.96 indicate C–C delocalized π bonds[47]. The BV(ELF$_\pi$)s for carbon–carbon bonds in **1**-S_0, **2**-S_0, **3**-S_0, and **2**-T_1 are in the range of 0.742–0.955 (Fig. 1b). A small span of BV(ELF$_\pi$) (ΔBV(ELF$_\pi$)) for C–C bonds is also an indicator of aromaticity[47]. As shown in Fig. 1b, the ΔBV(ELF$_\pi$)s in **2**-S_0 and **2**-T_1 are close to each other, indicating the adaptive aromaticity. In contrast, the ΔBV(ELF$_\pi$)s in **1**-T_1 is more than six times of that in **1**-S_0, close to that (0.764 in Supplementary Fig. 5) of benzene in the T_1 state, suggesting the antiaromaticity. The intermediate ΔBV(ELF$_\pi$) (0.474) of **3**-T_1 indicates its nonaromaticity in the T_1 state. The ELF$_\pi$ domains at the isovalue of 0.70 (Supplementary Fig. 6) reveal an electron delocalization on the carbon chains among **1**-S_0, **2**-S_0, **3**-S_0, and **2**-T_1. All these results are in line with those from NICS and ACID analyses.

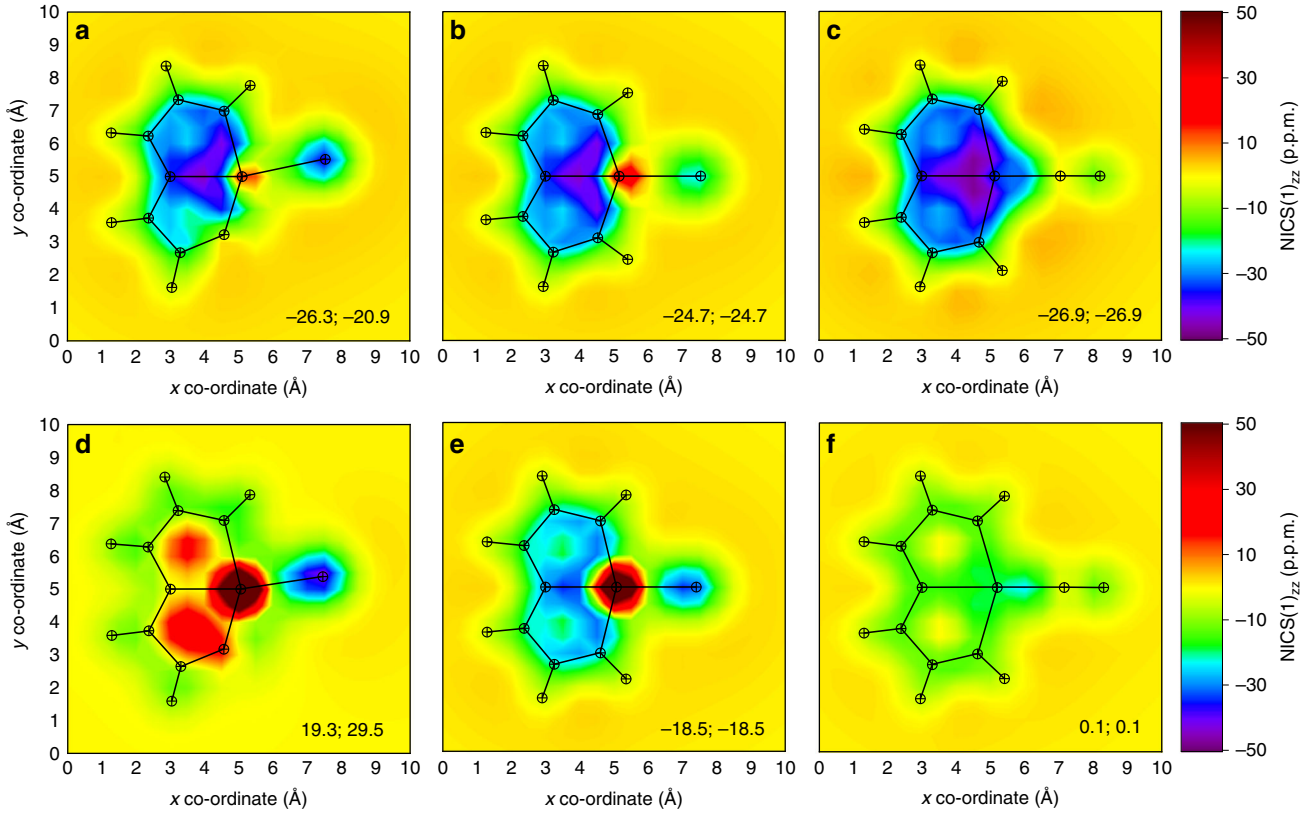

Fig. 2 NICS(1)$_{zz}$ grids for complexes **1**–**3** in the S_0 and T_1 states. Each grid covers a 10 × 10 Å square area parallel to molecular planes, with 0.5 Å resolution and 441 points in total (Supplementary Fig. 1). A fixed color scale (−50 to 50 p.p.m.) is applied to all grids for easy comparison. NICS(1)$_{zz}$ values calculated at the ring centers (upper ring; lower ring) are commented on the bottom-right of each grid. Projection of in-plane atomic positions are marked on the maps and connected accordingly with lines. **a**–**f** NICS(1)$_{zz}$ grids for **1**-S_0, **2**-S_0, **3**-S_0, **1**-T_1, **2**-T_1, and **3**-T_1

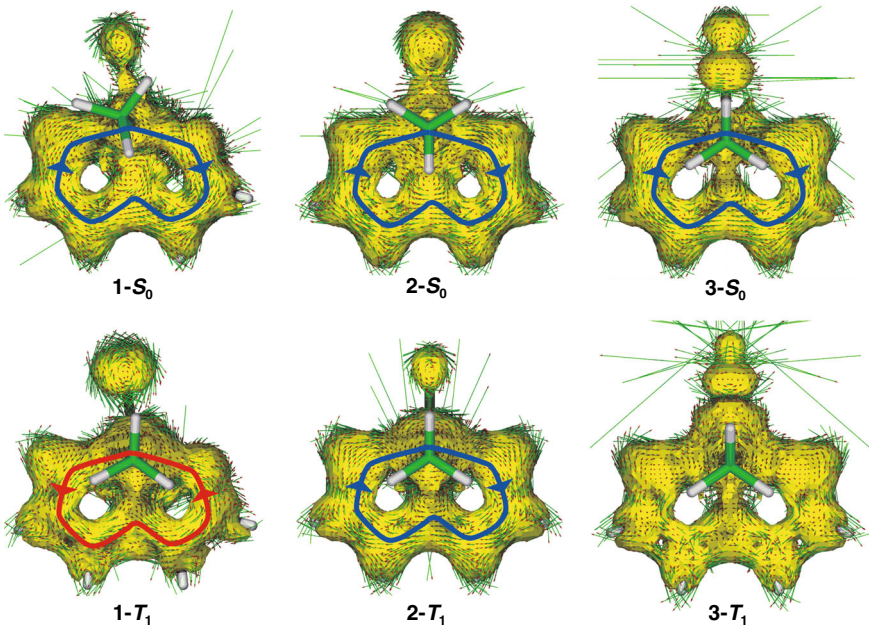

Fig. 3 ACID plots of complexes **1**-**3** in the S_0 and T_1 states. The molecular planes are placed perpendicular to the magnetic field vector. Small green arrows are computed current density vectors. The isovalue for the surfaces is 0.035 a.u. The paratropic/diatropic ring currents indicate antiaromaticity and aromaticity, respectively

Aromaticity analyses based on frontier molecular orbitals. To probe the origin of adaptive aromaticity in complex **2**, we analyzed its frontier molecular orbitals and compared them with the other two complexes (Fig. 4, Supplementary Figs. 7–9). As shown in Fig. 4, the highest occupied molecular orbital (HOMO) of complex **2** in the S_0 state is particularly similar to that of complex **1**. However, its lowest unoccupied molecular orbital (LUMO) is significantly different from that of complex **1**. For instance, the LUMO of complex **2** is mainly in-plane antibonding interaction between the metal *d* orbital and the *p* orbital (lone pair) of the chloride ligand, whereas the LUMO of complex **1** is mainly out-of-plane π-antibonding interaction between the metal center and carbon chain. For complex **3**, its HOMO is similar to the LUMO of complex **2**, whereas the LUMO is similar to that of complex **1**. In comparison with conventional organic aromatics, the excitation pattern of metallaaromatics in the T_1 state is more complicated and thus becomes less predictable because the formation of the T_1 state is not always out-of-plane $\pi\pi^*$ excitation. Specifically, the HOMO and LUMO of complex **1** are both out-of-plane π MOs, leading to a formation of the T_1 state by out-of-plane $\pi\pi^*$ excitation. Thus, its T_1 state follows Baird's rule and is antiaromatic. In sharp contrast, the T_1 state of complex **2** is formed by the electronic excitation from the out-of-plane HOMO to the in-plane LUMO of the ground state. As the highest singly occupied molecular orbital (HSOMO) is in-plane, its contribution to the out-of-plane π aromaticity is expected to be minor. Thus, it is understandable that complex **2** does not follow Baird's rule in terms of triplet-state aromaticity. Similarly, for complex **3**, the HOMO in the S_0 state is an in-plane π orbital. Its T_1 state is, therefore, not formed by out-of-plane $\pi\pi^*$ excitation. So complex **3** is not expected to follow Baird's rule in the T_1 state, too. All these qualitative analyses are also supported by ACID calculations on these key frontier molecular orbitals (Fig. 4).

When an occupied π bonding orbital in an aromatic species excites an electron to form the T_1 state, its contribution to the diatropic ring currents will be reduced, such as the HSOMO-1 of complexes **1**–**2** and benzene, as indicated by the ACID plots (Fig. 4). Meanwhile, even a single electron in an antibonding π orbital might have significant contribution to the paratropic ring currents, which is demonstrated here by the HSOMOs in the $\boldsymbol{T_1}$ state of **1**, **3**, and benzene (Fig. 4). The rest low-lying π orbitals are still doubly occupied and remain almost unchanged. Therefore, these orbitals are not discussed here. The aromaticity reversal in **1** could be ascribed to the reduced diatropic ring current of HSOMO-1 and newly generated significantly paratropic ring current of HSOMO, similar to those of benzene in the T_1 state. The aromaticity of **2** is slightly reduced in the T_1 state because its HSOMO is in-plane and the contribution to π aromaticity is negligible. The ignorable contribution by HSOMO of **2** was confirmed by further calculations on the radical formed by removing an electron from this orbital. As shown in Supplementary Fig. 10, the dicationic species **2′** is aromatic in the doublet state. As for **3**, there is no loss of electrons in the out-of-plane π bonding orbitals in the T_1 state, whereas the newly generated paratropic ring current of HSOMO neutralizes the diatropic ring current caused by almost unchanged π orbitals, leading to the nonaromaticity in the T_1 state of complex **3**. In a word, the in-plane LUMO of complex **2** plays a crucial role in the achievement of its aromaticity in the T_1 state, resulting in the first example of adaptive aromaticity.

Aromaticity analyses based on the spin density. In Baird's original paper, he pointed out that the π–π^* excitation tends to be "localized" within a subunit of a molecule[13]. For instance, the lowest triplet state of acenaphthylene has a larger contribution from excitation localized at an ethylenic bond than rather that delocalized across the entire π network[13]. In a recent study, we found that the localization of the spin density is found for antiaromatic species in the T_1 state, whereas triplet-state aromatic compounds have a tendency to delocalize their spin densities[41]. How about the population of the spin density in complexes **1**-$\boldsymbol{T_1}$, **2**-$\boldsymbol{T_1}$, **3**-$\boldsymbol{T_1}$, and **2′**? As shown in Fig. 5, different from our previous observation in main-group systems, the localization of the spin density is found for aromatic species **2**-$\boldsymbol{T_1}$ and **2′**, whereas the delocalization of the spin density for **1**-$\boldsymbol{T_1}$ and **3**-$\boldsymbol{T_1}$.

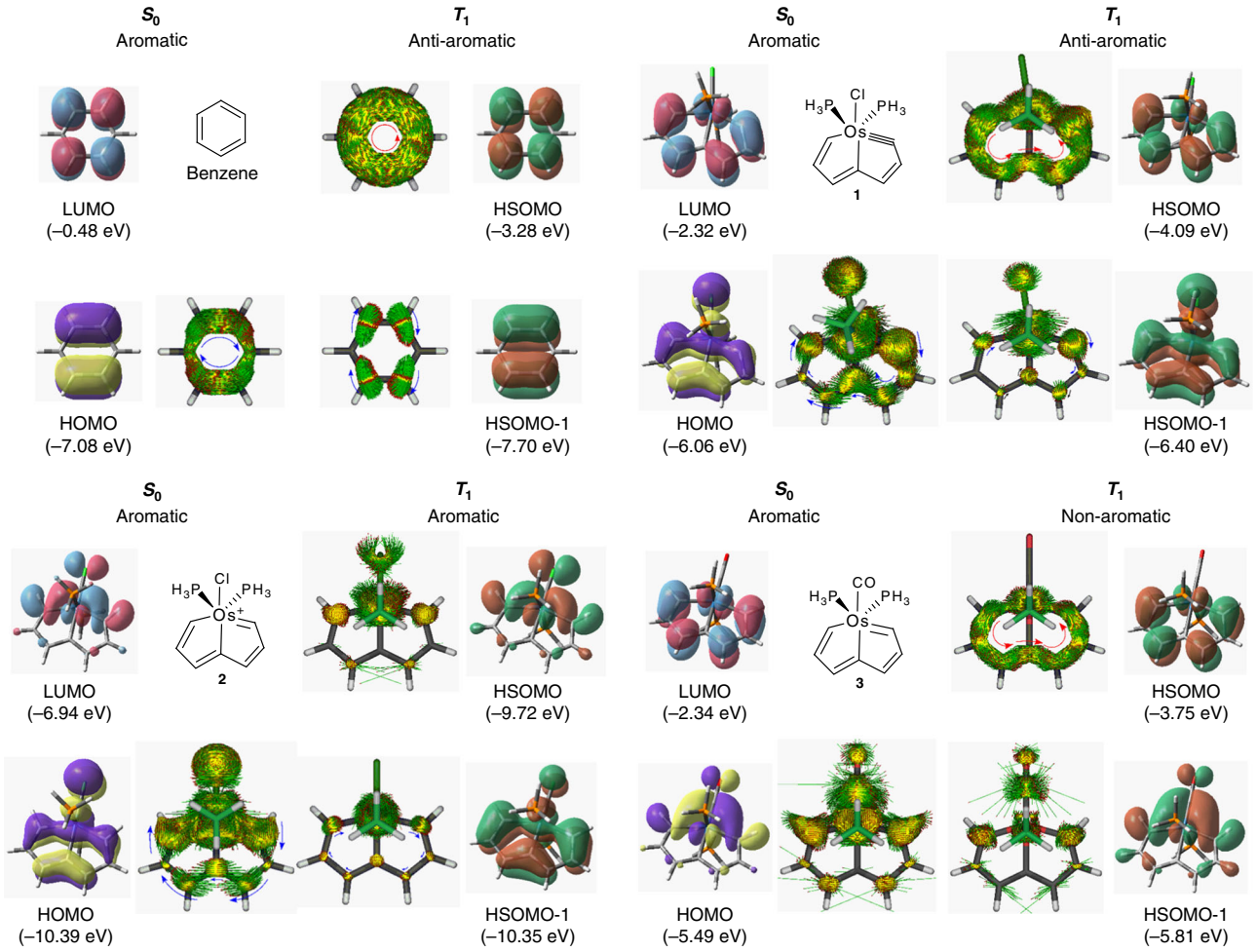

Fig. 4 ACID plots for individual molecular orbitals. Although all the listed MOs possess π character, the "π orbitals" we discussed in this study only refer to those anti-symmetric to the molecular plane. The isovalues for MO and ACID surfaces are 0.03 and 0.024 a.u., respectively. Despite the fact that benzene possesses two degenerate LUMOs and two degenerate HOMOs, we only take those consistent with the SOMOs (T_1) for demonstration

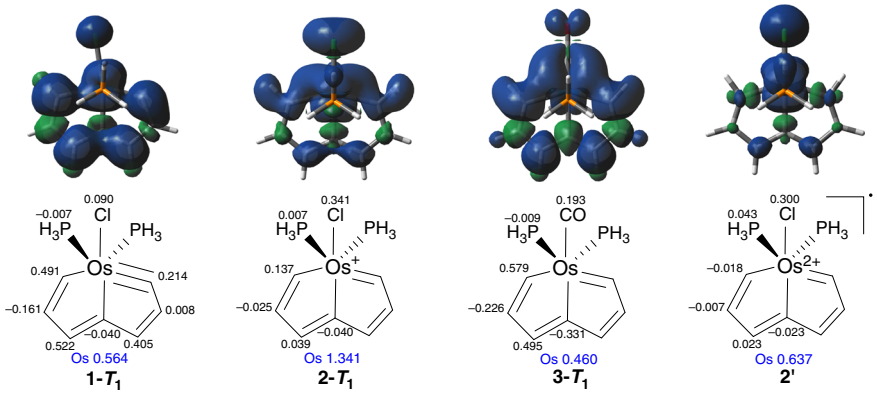

Fig. 5 Spin density analyses for open-shell species. Density surfaces are presented with an isovalue 0.001 a.u. Specific values of the spin density are given at individual atoms and key ligands. The "-" sign simply refers to the β-spin

Such a difference could be mainly attributed to the effect of transition metals and the character of their HSOMOs.

Adaptive aromaticity in 16e$^-$ osmapentalenes with bulky phosphines. To assure that the simplification of phosphorus ligands does not alter the nature of adaptive aromaticity in **2**, we examined two bulky ligands—trimethyl phosphine (PMe_3) and triphenyl phosphine (PPh_3), which are commonly used in experiments. The NICS(1)$_{zz}$ grids computed for 16e$^-$ osmapentalenes with these two ligands are basically same as those for the simplified model **2** (Supplementary Fig. 2), validating adaptive aromaticity concept concluded in this study.

Discussion

We have demonstrated that osmapentalene **2** is aromatic in both the S_0 and T_1 states, which is supported by various aromaticity

indices including NICS(1)$_{zz}$, ACID, HOMA, and ELF$_\pi$ analyses. In addition, osmapentalyne **1** follows Baird's rule and exhibits aromaticity reversal from the S_0 state to the T_1 state, indicating a "Dr. Jekyll and Mr. Hyde" split personality feature[48]. On the other hand, osmapentalenes **2** and **3** do not possess the out-of-plane $\pi\pi^*$ T_1 state, and thus are out of the scope of Baird's rule. Electronic structure analyses based on molecular orbital theory reveal a distinctive excitation pattern for the formation of the T_1 state of complex **2**, leading to the first example to achieve adaptive aromaticity, which has been rationalized by the ACID analyses. Thus, in-plane excitation rather than out-of-plane $\pi\pi^*$ is essential to achieve the adaptive aromaticity. Our findings highlight the importance of a transition metal in a rare excitation fashion to feature double "Dr. Jekyll" personality in the S_0 and T_1 states, potentially opening an avenue to design adaptive aromatics for photochemistry and molecular magnets.

Methods

Computational details. All the DFT calculations except fragment analyses were carried out with Gaussian 03 software package[49]. Geometric optimizations together with frequency calculations were performed at the (U)B3LYP level of theory. The 6-311++G(d,p) basis set was employed for C, H, and O atoms. For P, Cl, Os, and Ru atoms the pseudopotential basis set LANL2DZ was used, with polarization functions for P ($\zeta(d)$=0.340), Cl ($\zeta(d)$=0.514), and Os ($\zeta(f)$=0.886)[50,51], NICS calculations were carried out at (U)B3LYP-GIAO/6-311++G(d, p) level. The gauge invariant atomicorbitals (GIAO) and continuous set of gauge transformations (CSGT) methods were used to compute the NICS values and ACID plots, respectively. Fragment analyses (Supplementary Figs. 7–9) were performed using ADF (2017.104) program package at B3LYP/TZ2P level of theory[52,53], Zero-order regular approximation (ZORA) was applied for consideration of scalar relativistic effects. An auxiliary set of diffuse functions was included in the calculations. ELF$_\pi$ analyses were conducted using Multiwfn with wavefunctions obtained from geometry optimizations[54]. The ELF$_\pi$ bifurcation points were accurately located with the help of topology analysis implemented in Multiwfn, by searching critical points within spheres and using each nucleus in the molecule as sphere center in turn. Cartesian coordinates (Supplementary Table 2) of structures and high-resolution ACID plots (Supplementary Figs. 11–29) are provided in the Supplementary Information.

Data availability. All data generated or analyzed during this study are included in this published article (and its supplementary information files) and are available from the corresponding author upon reasonable request.

Received: 23 December 2017 Accepted: 27 February 2018
Published online: 05 April 2018

References

1. Hückel, E. Quantentheoretische beiträge zum benzolproblem. *Z. Phys.* **70**, 204–286 (1931).
2. Doering, W. V. E. & Detert, F. L. Cycloheptatrienylium oxide. *J. Am. Chem. Soc.* **73**, 876–877 (1951).
3. Dewar, M. J. S. A molecular orbital theory of organic chemistry—VIII. *Tetrahedron* **22**, 75–92 (1966).
4. Zimmerman, H. E. On molecular orbital correlation diagrams, the occurrence of Möbius systems in cyclization reactions, and factors controlling ground- and excited-state reactions. I. *J. Am. Chem. Soc.* **88**, 1564–1565 (1966).
5. Zimmerman, H. E. Möbius-Hückel concept in organic chemistry. Application of organic molecules and reactions. *Acc. Chem. Res* **4**, 272–280 (1971).
6. Heilbronner, E. Hückel molecular orbitals of Möbius-type conformations of annulenes. *Tetrahedron Lett.* **5**, 1923–1928 (1964).
7. Schleyer, P. v. R. Introduction: delocalization Pi and Sigma. *Chem. Rev.* **105**, 3433–3435 (2005).
8. Gleiter, R. & Haberhauer, G. *Aromaticity and Other Conjugation Effects*. (Wiley-VCH, Weinheim, 2012).
9. Ueda, M. et al. Energetics of Baird aromaticity supported by inversion of photoexcited chiral [4*n*]annulene derivatives. *Nat. Commun.* **8**, 346 (2017).
10. Papadakis, R. et al. Metal-free photochemical silylations and transfer hydrogenations of benzenoid hydrocarbons and graphene. *Nat. Commun.* **7**, 12962 (2016).
11. Ottosson, H. Organic photochemistry: Exciting excited-state aromaticity. *Nat. Chem.* **4**, 969–971 (2012).
12. Rosenberg, M., Dahlstrand, C., Kilså, K. & Ottosson, H. Excited state aromaticity and antiaromaticity: Opportunities for photophysical and photochemical rationalizations. *Chem. Rev.* **114**, 5379–5425 (2014).
13. Baird, N. C. Quantum organic photochemistry. II. Resonance and aromaticity in the lowest $^3\pi\pi^*$ state of cyclic hydrocarbons. *J. Am. Chem. Soc.* **94**, 4941–4948 (1972).
14. Aihara, J.-i. Aromaticity-based theory of pericyclic reactions. *B. Chem. Soc. Jpn.* **51**, 1788–1792 (1978).
15. Wan, P. & Krogh, E. Evidence for the generation of aromatic cationic systems in the excited state. Photochemical solvolysis of fluoren-9-ol. *J. Chem. Soc. Chem. Commun.* **4**, 1207–1208 (1985).
16. Gogonea, V., Schleyer, P.v. R. & Schreiner, P. R. Consequences of triplet aromaticity in 4*n*π-electron annulenes: Calculation of magnetic shieldings for open-shell species. *Angew. Chem. Int. Ed.* **37**, 1945–1948 (1998).
17. Sung, Y. M. et al. Reversal of Hückel (anti)aromaticity in the lowest triplet states of hexaphyrins and spectroscopic evidence for Baird's rule. *Nat. Chem.* **7**, 418–422 (2015).
18. Sung, Y. M. et al. Switching between aromatic and antiaromatic 1,3-phenylene-strapped [26]- and [28]hexaphyrins upon passage to the singlet excited state. *J. Am. Chem. Soc.* **137**, 11856–11859 (2015).
19. Cha, W. -Y. et al. Multifaceted [36]octaphyrin(1.1.1.1.1.1.1.1): deprotonation-induced switching among nonaromatic, Möbius aromatic, and Hückel antiaromatic species. *Chem. Commun.* **52**, 6076–6078 (2016).
20. Oh, J. et al. Aromaticity reversal in the lowest excited triplet state of archetypical mobius heteroannulenic systems. *Angew. Chem. Int. Ed.* **55**, 6487–6491 (2016).
21. Sung, Y. M. et al. A description of vibrational modes in hexaphyrins: Understanding the aromaticity reversal in the lowest triplet state. *Angew. Chem. Int. Ed.* **55**, 11930–11934 (2016).
22. Hong, Y. et al. The extension of Baird's rule to twisted heteroannulenes: Aromaticity reversal of singly and doubly twisted molecular systems in the lowest triplet state. *Angew. Chem. Int. Ed.* **56**, 2932–2936 (2017).
23. Möllerstedt, H., Piqueras, M. C., Crespo, R. & Ottosson, H. Fulvenes, fulvalenes, and azulene: Are they aromatic chameleons? *J. Am. Chem. Soc.* **126**, 13938–13939 (2004).
24. Ottosson, H. et al. Scope and limitations of Baird's theory on triplet state aromaticity: application to the tuning of singlet-triplet energy gaps in fulvenes. *Chem. -Eur. J.* **13**, 6998–7005 (2007).
25. Rosenberg, M., Ottosson, H. & Kilså, K. Influence of excited state aromaticity in the lowest excited singlet states of fulvene derivatives. *Phys. Chem. Chem. Phys.* **13**, 12912–12919 (2011).
26. Jorner, K. et al. Impact of ground- and excited-state aromaticity on cyclopentadiene and silole excitation energies and excited-state polarities. *Chem. -Eur. J.* **20**, 9295–9303 (2014).
27. Ayub, R., Bakouri, O. E., Jorner, K., Solà, M. & Ottosson, H. Can Baird's and Clar's rules combined explain triplet state energies of polycyclic conjugated hydrocarbons with fused 4*n*π- and (4*n* + 2)π-rings? *J. Org. Chem.* **82**, 6327–6340 (2017).
28. Fratev, F., Monev, V. & Janoschek, R. Ab initio study of cyclobutadiene in excited states: optimized geometries, electronic transitions and aromaticities. *Tetrahedron* **38**, 2929–2932 (1982).
29. Karadakov, P. B. Ground- and excited-state aromaticity and antiaromaticity in benzene and cyclobutadiene. *J. Phys. Chem. A* **112**, 7303–7309 (2008).
30. Feixas, F., Vandenbussche, J., Bultinck, P., Matito, E. & Solà, M. Electron delocalization and aromaticity in low-lying excited states of archetypal organic compounds. *Phys. Chem. Chem. Phys.* **13**, 20690–20703 (2011).
31. Zhu, C. et al. Stabilization of anti-aromatic and strained five-membered rings with a transition metal. *Nat. Chem.* **5**, 698–703 (2013).
32. Zhu, C. et al. Planar Mobius aromatic pentalenes incorporating 16 and 18 valence electron osmiums. *Nat. Commun.* **5**, 3265 (2014).
33. Mauksch, M. & Tsogoeva, S. B. Demonstration of "Möbius" aromaticity in planar metallacycles. *Chem. -Eur. J.* **16**, 7843–7851 (2010).
34. Wang, X., Zhu, C., Xia, H. & Zhu, J. Theoretical study on the stability and aromaticity of metallasilapentalynes. *Organometallics* **33**, 1845–1850 (2014).
35. An, K., Shen, T. & Zhu, J. Craig-Type Möbius aromaticity and antiaromaticity in dimetalla[10]annulenes: A metal-induced Yin-and-Yang pair. *Organometallics* **36**, 3199–3204 (2017).
36. Schleyer, P.v. R., Maerker, C., Dransfeld, A., Jiao, H. & Hommes, N. J. R.v. E. Nucleus-independent chemical shifts: A simple and efficient aromaticity probe. *J. Am. Chem. Soc.* **118**, 6317–6318 (1996).
37. Chen, Z., Wannere, C. S., Corminboeuf, C., Puchta, R. & Schleyer, P. v. R. Nucleus-independent chemical shifts (NICS) as an aromaticity criterion. *Chem. Rev.* **105**, 3842–3888 (2005).

38. Gershoni-Poranne, R. & Stanger, A. The NICS-XY-scan: identification of local and global ring currents in multi-ring systems. *Chem. -Eur. J.* **20**, 5673–5688 (2014).
39. Peeks, M. D., Claridge, T. D. & Anderson, H. L. Aromatic and antiaromatic ring currents in a molecular nanoring. *Nature* **541**, 200–203 (2017).
40. Fallah-Bagher-Shaidaei, H., Wannere, C. S., Corminboeuf, C., Puchta, R. & Schleyer, Pv. R. Which NICS aromaticity index for planar π rings is best? *Org. Lett.* **8**, 863–866 (2006).
41. Sun, H., An, K. & Zhu, J. Triplet state aromaticity: NICS criterion, hyperconjugation, and charge effects. *Chem. -Asian J.* **11**, 234–240 (2016).
42. Herges, R. & Geuenich, D. Delocalization of electrons in molecules. *J. Phys. Chem. A* **105**, 3214–3220 (2001).
43. Geuenich, D., Hess, K., Köhler, F. & Herges, R. Anisotropy of the induced current density (ACID), a general method to quantify and visualize electronic delocalization. *Chem. Rev.* **105**, 3758–3772 (2005).
44. Silvi, B. & Savin, A. Classification of chemical bonds based on topological analysis of electron localization functions. *Nature* **371**, 683–686 (1994).
45. Poater, J., Duran, M., Solà, M. & Silvi, B. Theoretical evaluation of electron delocalization in aromatic molecules by means of atoms in molecules (AIM) and electron localization function (ELF) topological approaches. *Chem. Rev.* **105**, 3911–3947 (2005).
46. Villaume, S., Fogarty, H. A. & Ottosson, H. Triplet-state aromaticity of 4*n*π-electron monocycles: analysis of bifurcation in the π contribution to the electron localization function. *ChemPhysChem.* **9**, 257–264 (2008).
47. Zhu, J., Dahlstrand, C., Smith, J. R., Villaume, S. & Ottosson, H. On the importance of Clar structures of polybenzenoid hydrocarbons as revealed by the π-contribution to the electron localization function. *Symmetry* **2**, 1653–1682 (2010).
48. Papadakis, R. & Ottosson, H. The excited state antiaromatic benzene ring: a molecular Mr Hyde? *Chem. Soc. Rev.* **44**, 6472–6493 (2015).
49. Frisch, M. J. et al. *Gaussian 03, Revision E.01*. (Gaussian, Inc., Wallingford CT, 2004).
50. Hay, P. J. & Wadt, W. R. Ab initio effective core potentials for molecular calculations. Potentials for potassium to gold including the outermost core orbitals. *J. Chem. Phys.* **82**, 299–310 (1985).
51. Huzinaga, S. Basis sets for molecular calculations. *Comput. Phys. Rep.* **2**, 281–339 (1985).
52. te Velde, G. et al. Chemistry with ADF. *J. Comput. Chem.* **22**, 931 (2001).
53. Fonseca Guerra, C., Snijders, J. G., te Velde, G. & Baerends, E. J. Towards an order-N DFT method. *Theor. Chem. Acc.* **99**, 391 (1998).
54. Lu, T. & Chen, F. Multiwfn: a multifunctional wavefunction analyzer. *J. Comput. Chem.* **33**, 580–592 (2012).

Acknowledgements

Financial support by the Top-Notch Young Talents Program of China, the National Science Foundation of China (21573179) and the Program for Changjiang Scholars and Innovative Research Team in University (IRT1263) is gratefully acknowledged. We thank Prof. Henrik Ottosson at Uppsala University and Prof. Sason Shaik at the Hebrew University of Jerusalem for their suggestions and discussion.

Author contributions

J.Z. conceived and supervised the project. D.C. and J.Z. performed theoretical calculations. D.C. drafted the manuscript and J.Z. revised it. J.Z., D.C., T.S. and K.A. discussed the results and commented on the manuscript.

Additional information

Supplementary information accompanies this paper at https://doi.org/10.1038/s42004-018-0018-y.

Competing interests: The authors declare no competing interests.

Reprints and permission information is available online at http://npg.nature.com/reprintsandpermissions/

Publisher's note: Springer Nature remains neutral with regard to jurisdictional claims in published maps and institutional affiliations.